# Design of Flexible Dual-Band Tree Fractal Antenna for Wearable Applications

**Aya N. Alkhafaji[1, *], Sinan M. Abdulsatar[2], and Jawad K. Ali[1]**

**Abstract**—A dual-band flexible monopole antenna for wearable applications is presented. The antenna structure is built based on tree-shaped fractal geometry. The suggested antenna is printed on Rogers RT5870, a semi-flexible material with a relative dielectric constant and loss tangent of 2.33 and 0.0012, respectively. According to the results, the proposed antenna achieves dual impedance bandwidth ranging from 1.72 to 1.88 GHz for the lower band and 5.1 to 5.33 GHz for the upper band. The simulated results show that the fractional impedance bandwidths and realized gains of the antenna are 8.9/4.8% and 1.47/5.67 dBi for the 1.81/5.2 GHz, respectively. The antenna's performance under various bending scenarios has also been demonstrated at both resonant frequencies. The overall size of the proposed antenna is about $45 \times 41 \times 0.25\,\text{mm}^3$. The antenna shows good performance to be a candidate for wearable applications.

## 1. INTRODUCTION

Wearable electronic devices have attracted attention due to their potential uses in various fields, such as medical treatment, trace tracking, military applications, entertainment, and emergency rescue operations [1–3]. Wearable antenna plays a crucial role in signal transmission in the above systems, providing high flexibility and compatibility with other components. The antenna is responsible for wireless communication between on-body sensors and other on-/off-body devices in these wearable systems [4, 5]. Fractal antenna theory is a relatively recent field in antenna research. Fractals are patterns of self-similarity inspired by natural phenomena such as coastlines, mountains, and clouds [6–8]. Antenna designs can use fractals to achieve multiband resonant behavior and size miniaturization [6–12]. Self-similarity has been used in constructing multiband arrays and is helpful in the design of multi-frequency antennas. Many fractal forms have been used to construct wearable antennas, including Hilbert curve, Sierpinski gasket, Koch snowflake, Cantor's comb, Mandelbrot set, and Fern Fractal leaf [13–18].

In the past, many types of wearable antennas have been suggested. Fractal antennas have been proposed by [19] and [20] for wearable applications. However, the two designed antennas are not suitable for integrating with compact RFID wearable devices. Large-sized fractal antennas with full ground plane [21, 22] are more sensitive to deformations. Other fractal antennas are proposed by [23] and [24], where these designs provide a complex geometry. In [25], a monopole tree fractal antenna consists of a patch element mounted on an isotropic dielectric layer over a truncated ground plane for different wireless applications. However, the overall dimensions of the antenna are too large to be used in any compact environment. In [26], a square microstrip fractal antenna operating at a multiband between 1.7 and 7.4 GHz is designed; however, the antenna has narrow fractional bandwidth.

\* Corresponding author: Aya N. Alkhafaji (a.n_1991@yahoo.com).
[1] Electrical Engineering Department, University of Technology-Iraq, Baghdad, Iraq. [2] Communication Engineering Department, University of Technology-Iraq, Microwave Research Group, Baghdad, Iraq.

The presented antenna is designed according to fractal geometry due to the pioneer features of this geometry, which makes it desirable in the field of antenna design in terms of multiband and size reduction. In addition, wearable antennas preferably have features so that they can be embedded within tissue arrangement, which makes this antenna very convenient in textile antennas.

The paper is arranged as follows. Section 2 introduces the nature of tree fractal. Section 3 discusses the antenna design and modeling. Section 4 presents a parametric study. Section 5 shows the antenna performance and simulation results. Section 6 offers the effect of bending on the dual-bands, followed by Section 7, which includes the conclusion.

## 2. FRACTAL NATURE OF THE TREE

In general, a fractal is an object that starts with a simple geometry and makes a given number of scaled duplicates of the initial object at each iteration. The geometry discussed in this paper is a fractal tree that is self-similar. The method used to create trees here begins with a trunk and allows one of its ends to branch off in two directions. Each of these branches is permitted to branch out again in the following iteration stage, and the process is repeated indefinitely, as shown in Figure 1 [27].
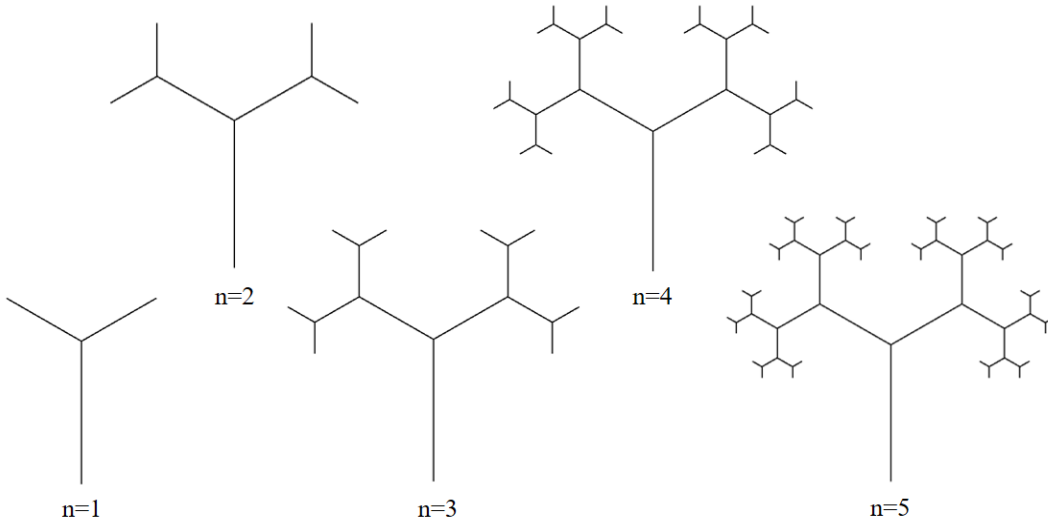


**Figure 1.** Various fractal binary tree iterations.

The primary objective of this study is to verify the theory developed about the link between antenna resonance characteristics and the fractal dimension of the geometry. As a result, two generalizations to basic geometry are attempted in this paper. The first step is to change the angle ($\theta$) of the branches (angular separation of the branches at every iteration stage). The second method involves varying the scaling ratio ($r_{sc}$) (relative lengths of the branch in one stage relative to the next). These are depicted in Figures 2 and 3. It should be remembered that after the initial branching, the geometry can be created using a recursive process in both circumstances. To make fractal property computations easier, we propose using only line segments for all branches of the geometry. Unlike Mandelbrot's, the tree structure employed here does not consider the width of the component segments.

We can change the scaling ratio between the lengths of the trunk and branches. The transformations necessary to obtain branches of the geometry, in this case, are as follows in (1) and (2):

$$W_1 \begin{pmatrix} x \\ y \end{pmatrix} = \begin{bmatrix} \dfrac{1}{r_{sc}} \cos\theta & -\dfrac{1}{r_{sc}} \sin\theta \\ \dfrac{1}{r_{sc}} \sin\theta & \dfrac{1}{r_{sc}} \cos\theta \end{bmatrix} \begin{pmatrix} x \\ y \end{pmatrix} + \begin{pmatrix} 0 \\ 1 \end{pmatrix} \qquad (1)$$
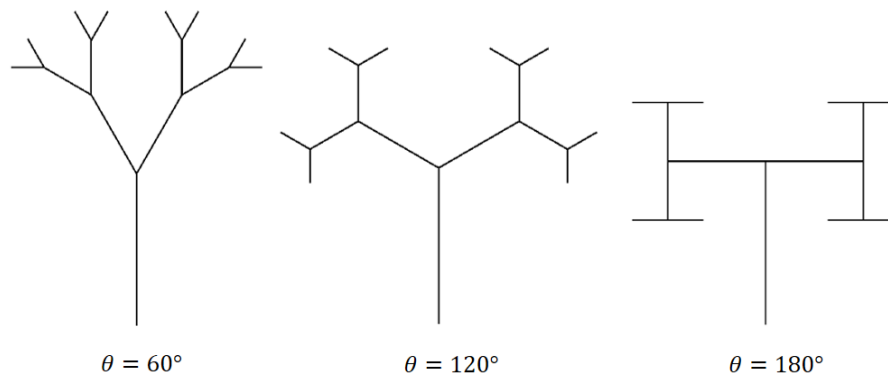
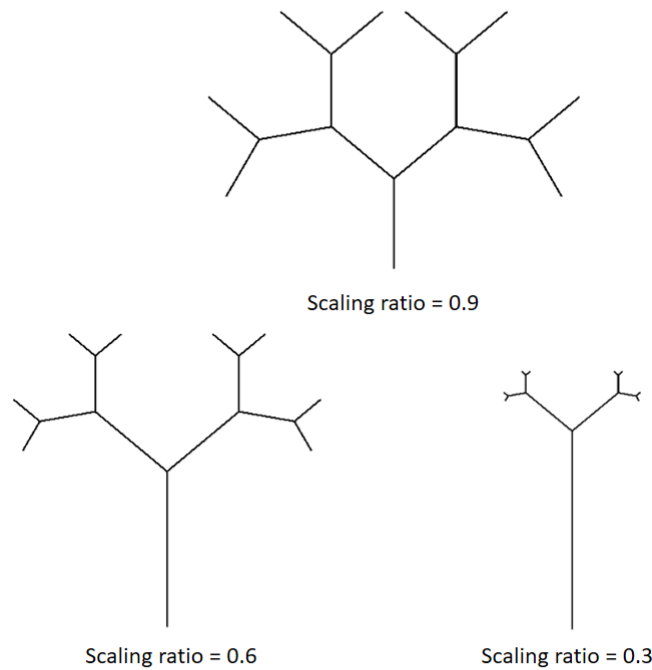**Figure 2.** Different branching angles in the third iterated fractal tree.



**Figure 3.** Binary trees with different scaling ratios in the third iteration.

$$W_2 \begin{pmatrix} x \\ y \end{pmatrix} = \begin{bmatrix} \dfrac{1}{r_{sc}} \cos\theta & \dfrac{1}{r_{sc}} \sin\theta \\ \dfrac{1}{r_{sc}} \sin\theta & \dfrac{1}{r_{sc}} \cos\theta \end{bmatrix} \begin{pmatrix} x \\ y \end{pmatrix} + \begin{pmatrix} 0 \\ 1 \end{pmatrix} \quad (2)$$

## 3. ANTENNA DESIGNING AND MODELING

A monopole antenna with a tree-shaped fractal component, a microstrip feed line, and a partial ground plane is suggested. The design procedure for the tree-shaped fractal antenna is shown in Figure 4. The basic unit of the tree-shaped fractal structure is a V-shaped metal strip (Iteration 1) with the length $y$ and width $x$, which are illustrated in Figure 4(a). In Figure 4(b), the length of the V-shaped unit cell ($y$) is scaled by factor $r_{sc}$, where $r_{sc}$ is the scale factor with a value ranging from 0 to 1 (Iteration 2). The same procedure is applied to Iteration 3 and Iteration 4 to form the tree-shaped fractal structure,
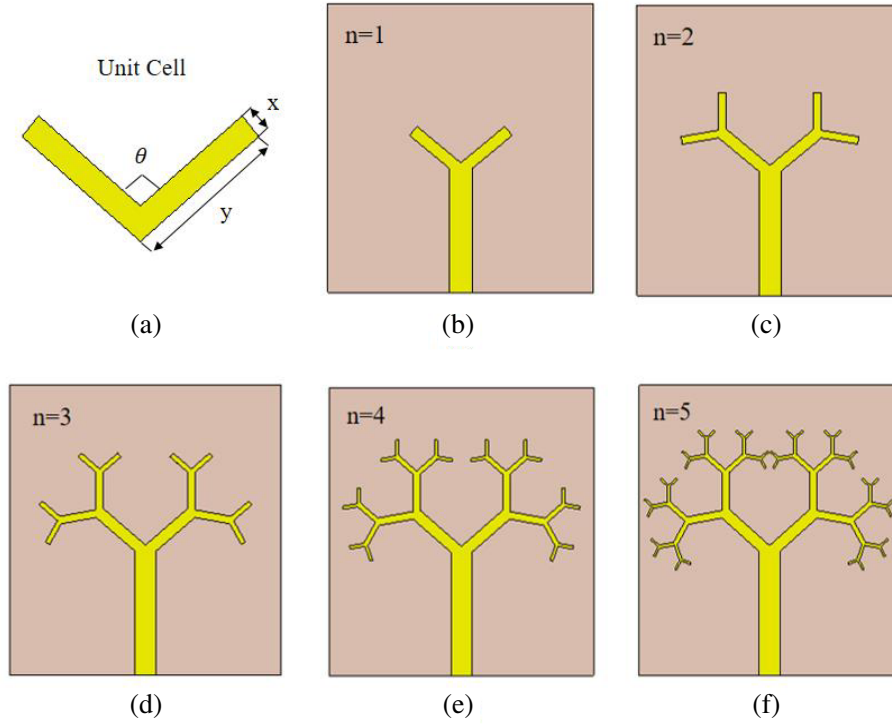
**Figure 4.** Evolution of the proposed antenna: (a) V-shaped unit cell, (b) Iteration 1, (c) Iteration 2, (d) Iteration 3, (e) Iteration 4 (proposed antenna) and (f) Iteration 5.
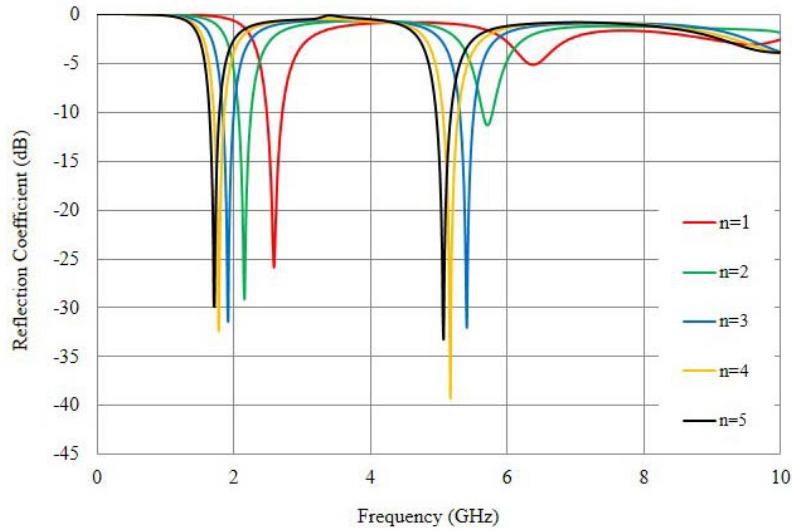


**Figure 5.** Simulated reflection coefficient of different iteration for the tree-shaped fractal-antenna structures.

as depicted in Figures 4(c) and (d). The unit cell's length can be calculated based on (3), where $n$ is the number of iterations in the fractal

$$y_n = r_{sc}^{n-1} y \quad n\ 1, 2, 3, \dots \tag{3}$$

The simulation results of the operating frequency, bandwidth, and reflection coefficients of the proposed tree-shaped fractal antenna's five first iterations are shown in Figure 5 and Table 1, where

**Table 1.** Simulation results of each patch iteration.

| Antennas | Operating frequency (GHz) | Bandwidth (MHz) | Reflection coefficient (dB) |
|---|---|---|---|
| $n1$ | 2.59 | 230.11 | $-25.9$ |
| $n2$ | 2.16/5.71 | 188.12/147.45 | $-29.1/-11.3$ |
| $n3$ | 1.92/5.40 | 167.22/209.48 | $-31.09/-31.88$ |
| $n4$ | 1.81/5.20 | 157.51/231.72 | $-32.0/-34.2$ |
| $n5$ | 1.71/5.07 | 148.31/222.24 | $-29.3/-34.0$ |

**Table 2.** Dimensions of the antenna.

| Parameter | Value (mm) | Parameter | Value (mm) |
|---|---|---|---|
| $x$ | 2 | $lg$ | 1 |
| $y$ | 12 | $W$ | 41 |
| $lt$ | 19.2 | $L$ | 45 |
| $wt$ | 3.4 | $r_{sc}$ | 0.65 |

$r_{sc} = 0.65$, $x = 2$ mm, and $y = 12$ mm. The angle between branches ($\theta$) is kept at $100°$. It has been noted that the proposed design resonates at a frequency of $2.59$ GHz in Iteration 1. In Iteration 2, a new resonant frequency of $5.71$ GHz is achieved. It could be seen that the resonant frequencies decrease from $2.59$ to $1.71$ GHz and $5.71$ to $5.07$ GHz for the lower and upper bands when $n$ fluctuates between 1 and 5. After four iterations, the proposed design is achieved, as shown in Figure 6. Table 2 shows the suggested design's optimal parameters. The suggested antenna is built on a semi-flexible Rogers RT5870 substrate with a relative permittivity ($\varepsilon_r$) of 2.33, loss tangent ($\tan\delta$) of 0.0012, and thickness ($h$) of $0.25$ mm. A transmission line feed with a length ($lt$) of $19.2$ mm and width ($wt$) of $0.8$ mm was used to feed the proposed antenna. On the backside of the substrate, a partial ground plane with a size of $41 \times 1$ mm$^2$ is included.



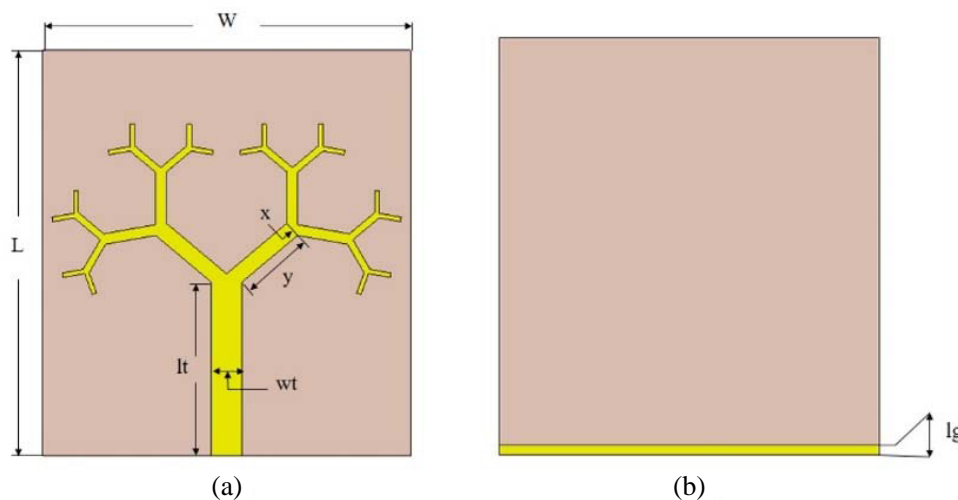(a)                                        (b)

**Figure 6.** The proposed antenna geometry and dimensions: (a) Top view and (b) bottom view.

## 4. PARAMETRIC STUDY

The parametric analysis was carried out to provide complete information regarding the antenna design. Only one parameter was varied at any time, and others were kept fixed. The dimensions and electrical properties of an antenna vary depending on the radiating patch and ground. As a result, the antenna's performance characteristics are altered. The antenna performance has been analyzed using a variety of parametric studies.

### 4.1. The Influence of the Parameter $y$

The effect of changing the length of the V-shaped unit cell ($y$) on the reflection coefficient characteristics is shown in Figure 7. The center of the lower and higher resonance bands shifts toward lower frequencies as the value of $y$ is increased from 9 to 12 mm. The antenna's upper resonant bandwidth is more extended than its lower one. As a result, an optimum value of 12 mm was considered in the proposed prototype.
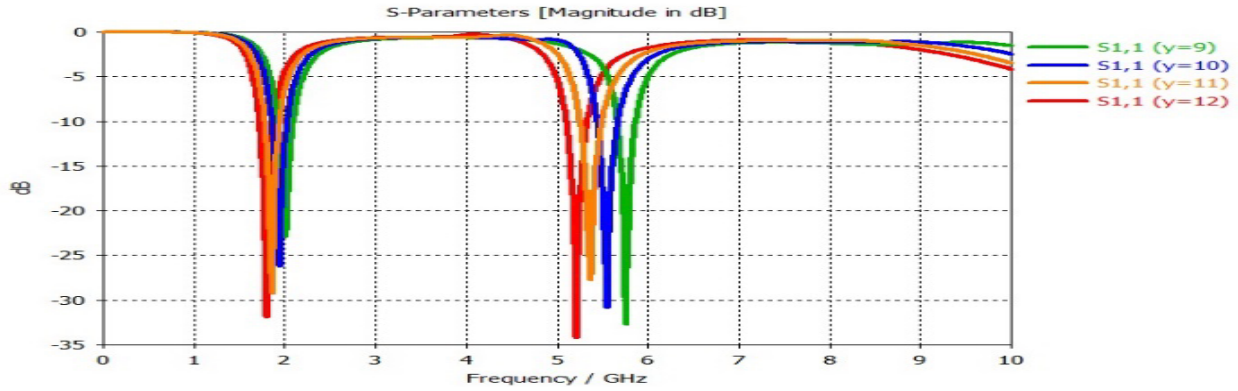


**Figure 7.** Simulations of the proposed antenna's reflection coefficients for various of the parameter $y$.

### 4.2. The Influence of the Parameter $r_{sc}$

Figure 8 shows the effect of variation on $r_{sc}$. The variation in $r_{sc}$ had a significant impact on the reflection coefficient performance as it varies from 0.55 to 0.75. A higher $r_{sc}$ leads to a more inductive impedance of each unit cell and, as a result, the more inductive input impedance of the antenna for a fixed $x$ in (3). So, raising $r_{sc}$ lowers the resonance frequency, as shown in Figure 8.
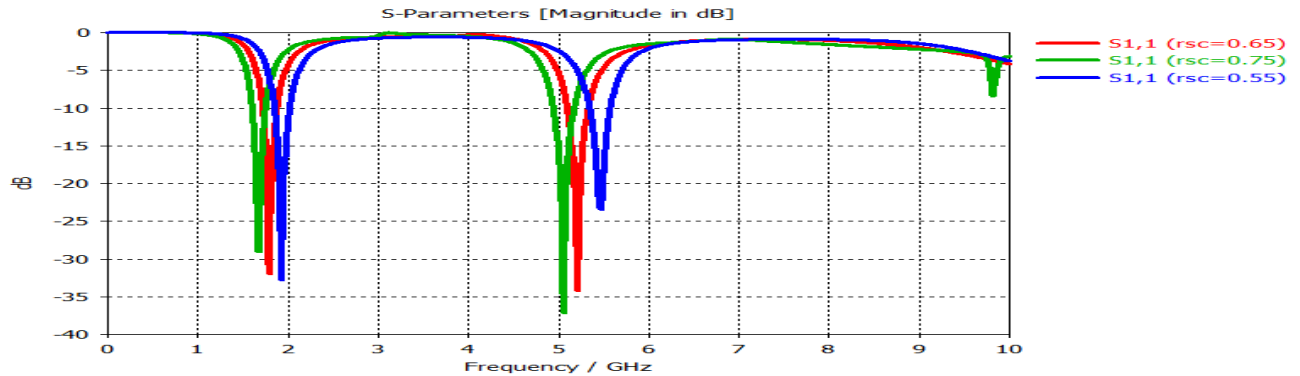


**Figure 8.** Simulations of the proposed antenna's reflection coefficients for various of the parameter $r_{sc}$.

### 4.3. The Influence of the Parameter $\theta$

The reflection coefficient performance for various values of $\theta$ is given in Figure 9. By taking angle variation from $90°$ to $120°$, the antenna provides dual-band reflection coefficient resonant responses with interesting features. The resonance frequency is shifted towards higher frequencies when the angle of $\theta$ has been increased. It was clear that the performance of the proposed design was far better at $\theta = 100°$.
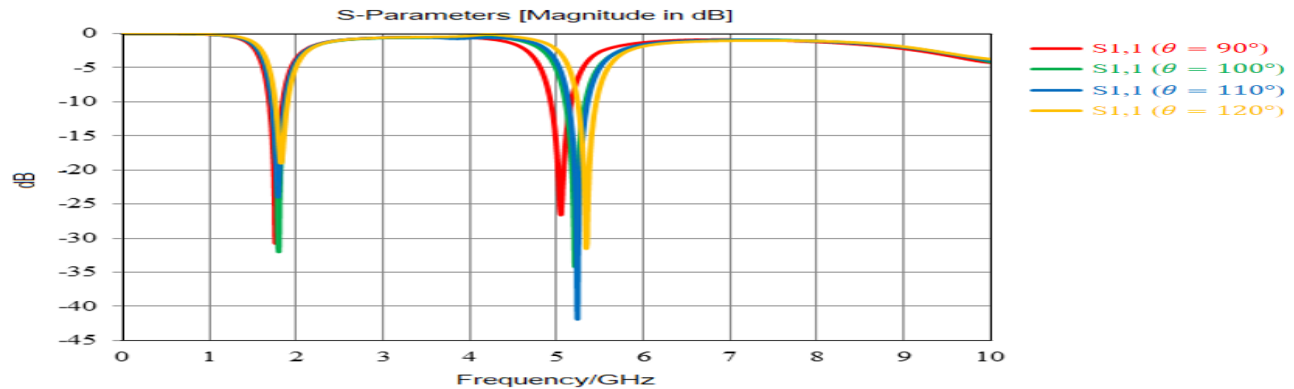
**Figure 9.** Simulations of the proposed antenna's reflection coefficients with different values of the branching angle $(\theta)$.

### 4.4. The Influence of the Parameter $lg$

Figure 10 illustrates the reflection coefficient responses of the proposed antenna with the ground plane length as a parameter at a sweep frequency of $(1–10)$ GHz. The ground plane is changed from $1$ mm to $10$ mm in $3$ mm steps, with a more significant influence on the higher resonant band than the lower band. The antenna achieves dual-band reflection coefficient resonant response matching with wearable frequency bands of $1.8$ GHz and $5.2$ GHz when the ground plane length $(lg)$ is $1$ mm.
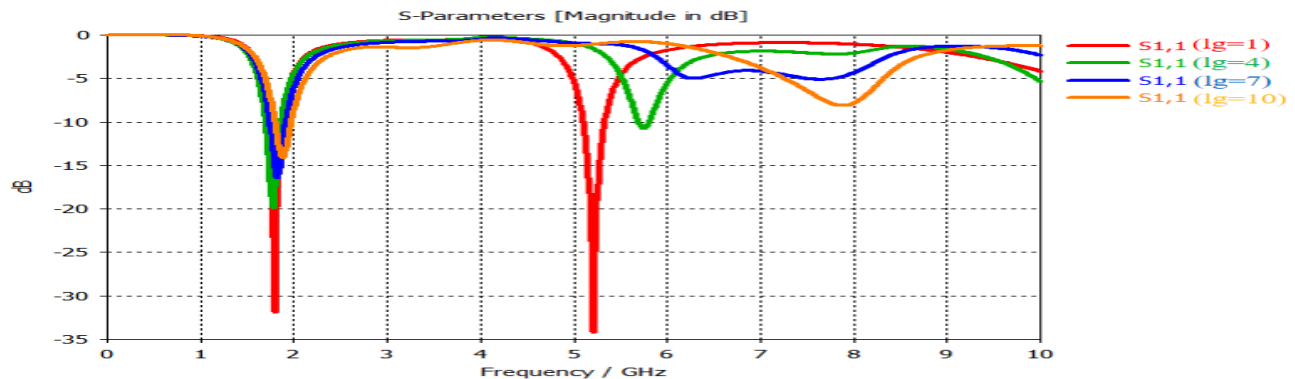
**Figure 10.** Simulations of the proposed antenna's reflection coefficients for different values of the ground plane length $(lg)$.

## 5. RESULTS AND DISCUSSION

CST Microwave Studio Software 2019 was used to develop and simulate the whole model. The suggested antenna's performance parameters, such as the reflection coefficient, gain, impedance bandwidth, and radiation pattern, have been determined. Figure 11 shows the simulated reflection coefficient $|S_{11}|$. The
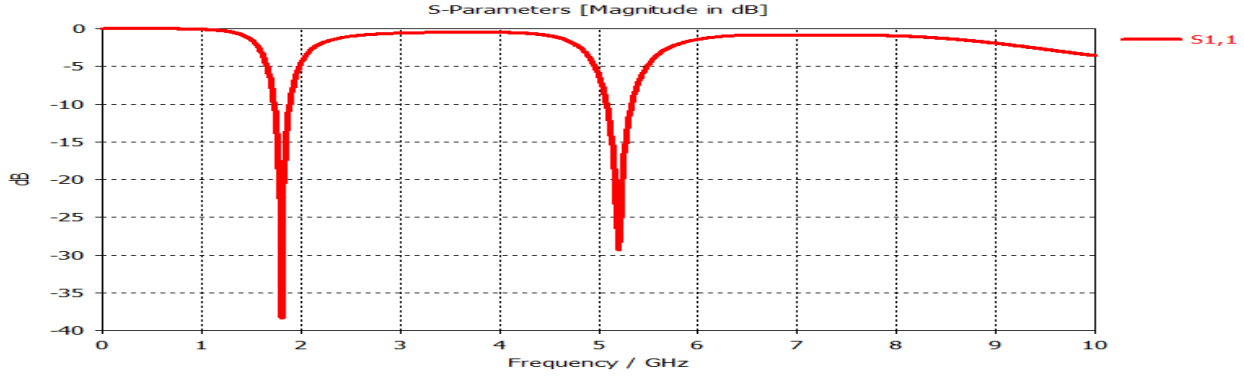
**Figure 11.** The $S_{11}$ curve of the tree-shaped fractal antenna.

lower and upper bands' impedance bandwidths ($|S_{11}| < -10$ dB) are 8.9% (1.72–1.88 GHz) and 4.8% (5.08–5.33 GHz), respectively.

The current distribution of the proposed antenna is as shown in Figure 12 for frequency bands 1.81 GHz and 5.2 GHz. At 1.81 GHz, it can be seen that the current is concentrated near the feed line and on the V-shaped unit cell of the tree-shaped fractal antenna, as shown in Figure 12(a). At 5.2 GHz, the surface current distribution is mainly concentrated at the V-shaped unit cell of $1^{st}$ and $2^{nd}$ iterations. In contrast, weak current distributions are concentrated near the edges at $3^{rd}$ and $4^{th}$ iterations as depicted in Figure 12(b).
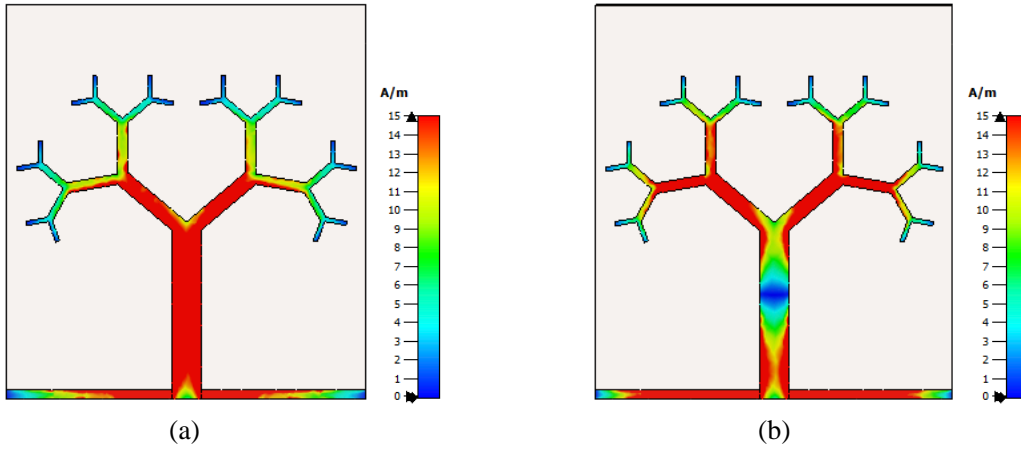


(a)        (b)

**Figure 12.** The current distribution of the proposed antenna at: (a) 1.81 GHz and (b) 5.2 GHz.

The simulated far-field radiation patterns for the total electric field in the two planes Phi = 0° and Phi = 90° at the center frequencies of the two resonant bands are shown in Figure 13. At 1.81 GHz, the antenna seems to have an omnidirectional pattern in the Phi = 0° and a half wavelength dipole-like pattern in the Phi = 90° as illustrated in Figure 13(a). Meanwhile, the antenna has an omnidirectional pattern in Phi = 0° and a directional pattern in Phi = 90° at the higher frequency of 5.2 GHz, as shown in Figure 13(b). The realized gain and efficiency of the antenna are 1.47/5.67 dBi and 98.2/95.7% for the 1.81/5.2 GHz bands, respectively.

A comparison of the performance of several existing works with the proposed antenna is presented in Table 3. In comparisons with listed wearable antennas, the proposed tree fractal antenna provides size reduction which makes the antenna suitable for wearable applications.

The proposed antenna was constructed as illustrated in Figure 14 and experimentally verified. Figure 15 shows the comparison between the measured and simulated results for the antenna's reflection coefficient.
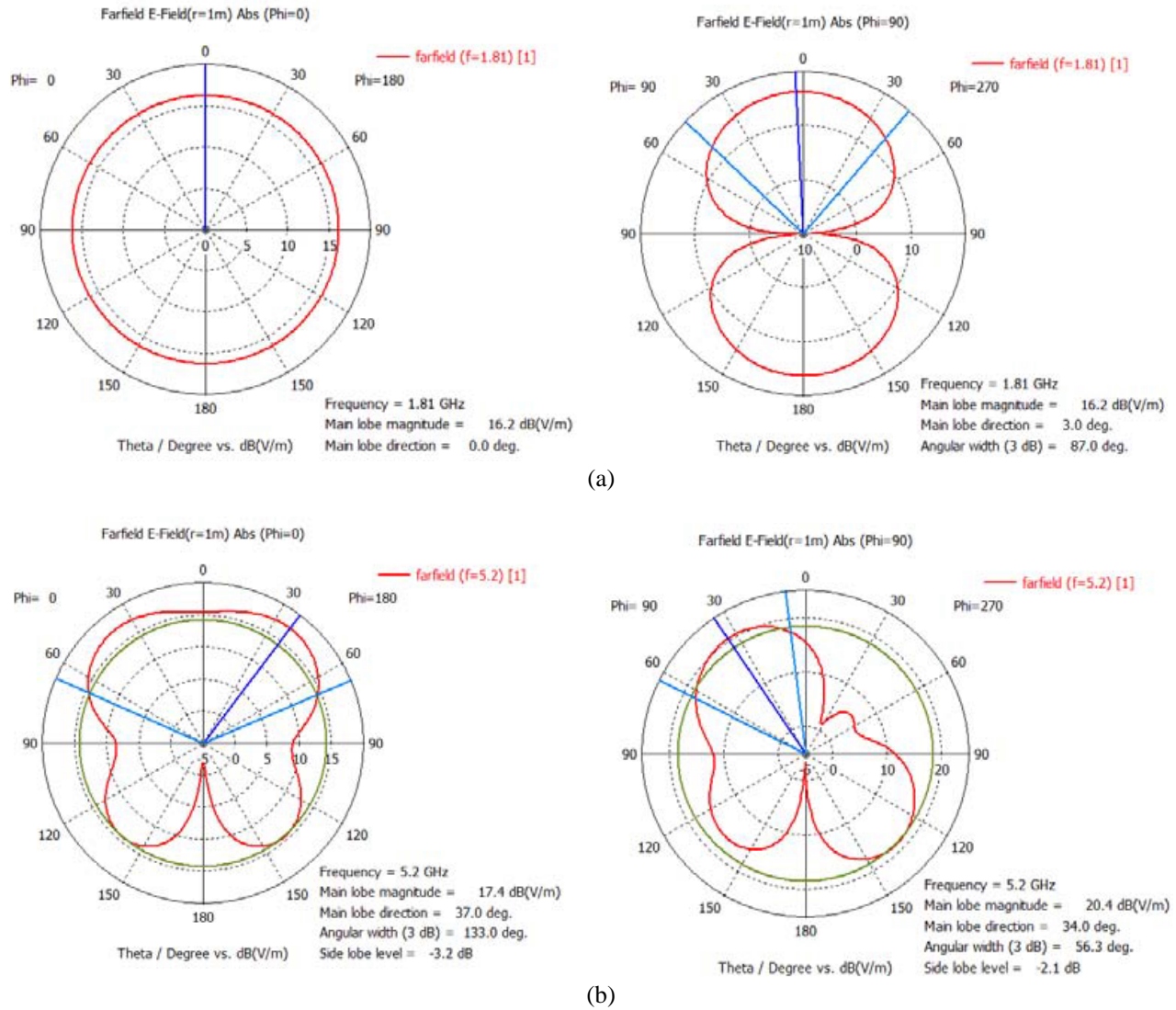
**Figure 13.** The 2D radiation patterns of the antenna for (phi = 0°) and (phi = 90°) at (a) 1.81 GHz, and (b) 5.2 GHz.
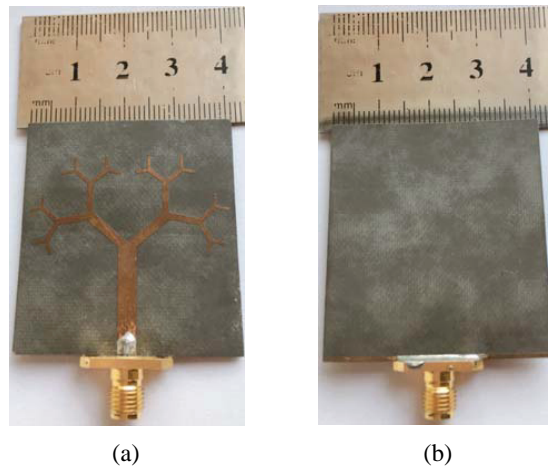


**Figure 14.** A photo of the manufactured proposed antenna.

**Table 3.** Comparison between the proposed antenna and some other reported works.

| Ref. | No. of bands | Relative permittivity $(\varepsilon_r)$ | Substrate type | Antenna configuration | Bandwidth frequency range, resonant frequency (GHz) | Gain (dBi) | Antenna size (mm$^3$) |
|------|------|------|------|------|------|------|------|
| [28] | single | 1.6 | Jeans | Microstrip patch antenna | 2.1–2.6, 2.45 | 2 | $90 \times 70 \times 1.57$ |
| [29] | single | 3.4 | Polyimide Film | Star-shaped patch antenna | 2.45 | 3.4 | $75 \times 50 \times 0.8$ |
| [30] | quad | 1.39 | Polyester cloth | V-shaped slot antenna | 1.70–2.01, 1.8<br>2.39–2.50, 2.4<br>3.59–3.70, 3.6<br>5.41–5.65, 5.5 | 4.91<br>7.84<br>2.58<br>4.12 | $70 \times 70 \times 2$ |
| [31] | dual | 3.5 | Kapton (polyimide) | Printed monopole antenna | 1.8–2.45<br>5.15–5.825 | 1.05<br>3.12 | $58 \times 40 \times 0.13$ |
| Proposed work | dual | 2.3 | Rogers RT5870 | Tree-shaped fractal antenna | 1.73–1.89, 1.81<br>5.08–5.33, 5.2 | 1.41<br>4.42 | $41 \times 45 \times 0.25$ |
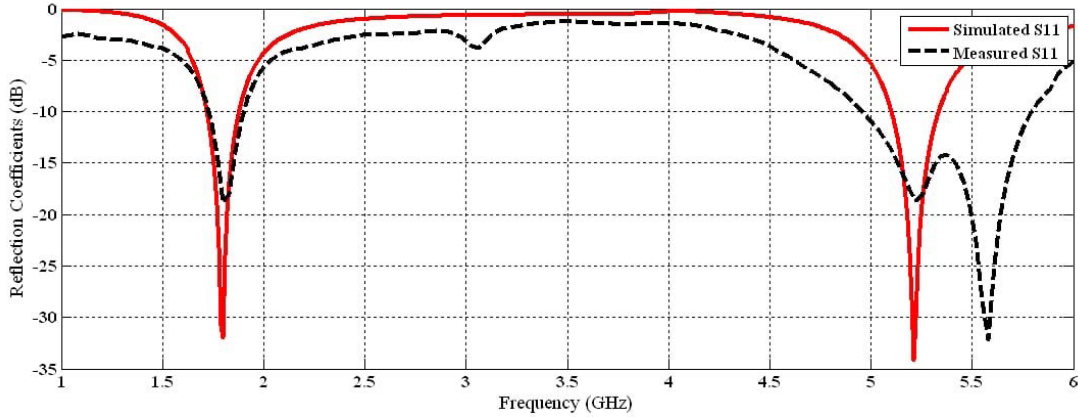


**Figure 15.** Simulated and measured results of the proposed antenna.

    A reasonable agreement is observed especially in the lower band. On the other hand, it can be seen that the measured upper band reflection coefficient has a bandwidth that is wider than the simulated one. The measured values range from 4.95 to 5.79 GHz with a bandwidth of 840 MHz (15.6%), while the simulated values range from 5.1 to 5.33 GHz with a bandwidth of 230 MHz (4.8%). This might be caused by the substrate material's lossy properties. Furthermore, the $S_{11}$ values in both bands are almost equivalent to $-18$ dB. The results are summarized in Table 4.

**Table 4.** A comparison of the simulation and measurement results.

|  | Simulated | | Measured | |
|------|------|------|------|------|
| Frequency (GHz) | 1.8 | 5.2 | 1.8 | 5.2 |
| $S_{11}$ (dB) | $-33$ | $-34.8$ | $-18.84$ | $-18.61$ |
| $f_o$ (GHz) | 1.8 | 5.2 | 1.8 | 5.37 |
| BW (MHz) | 160 | 230 | 170 | 840 |

## 6. A STUDY OF THE BENDING DEFORMATION

This section uses simulation results to investigate the consequences of the antenna when it is bent in free space. The proposed antenna was bent around a cylinder at different radii ($r$) to ensure robustness against bending scenarios.
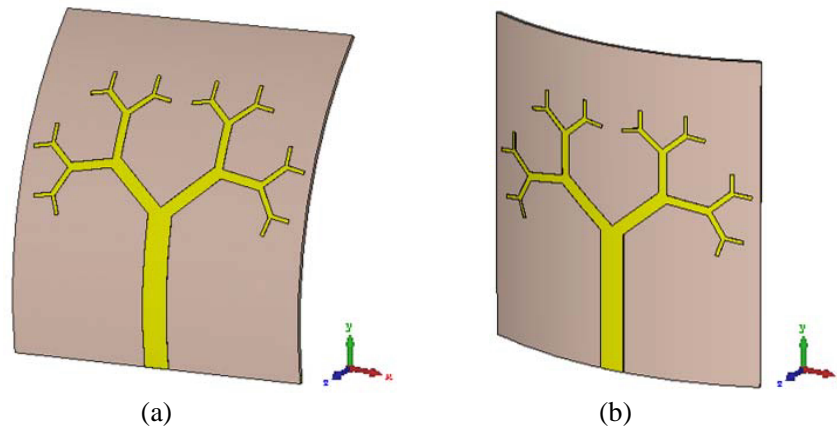


(a)          (b)

**Figure 16.** The proposed antenna while bending at: (a) $x$-axis and (b) $y$-axis.
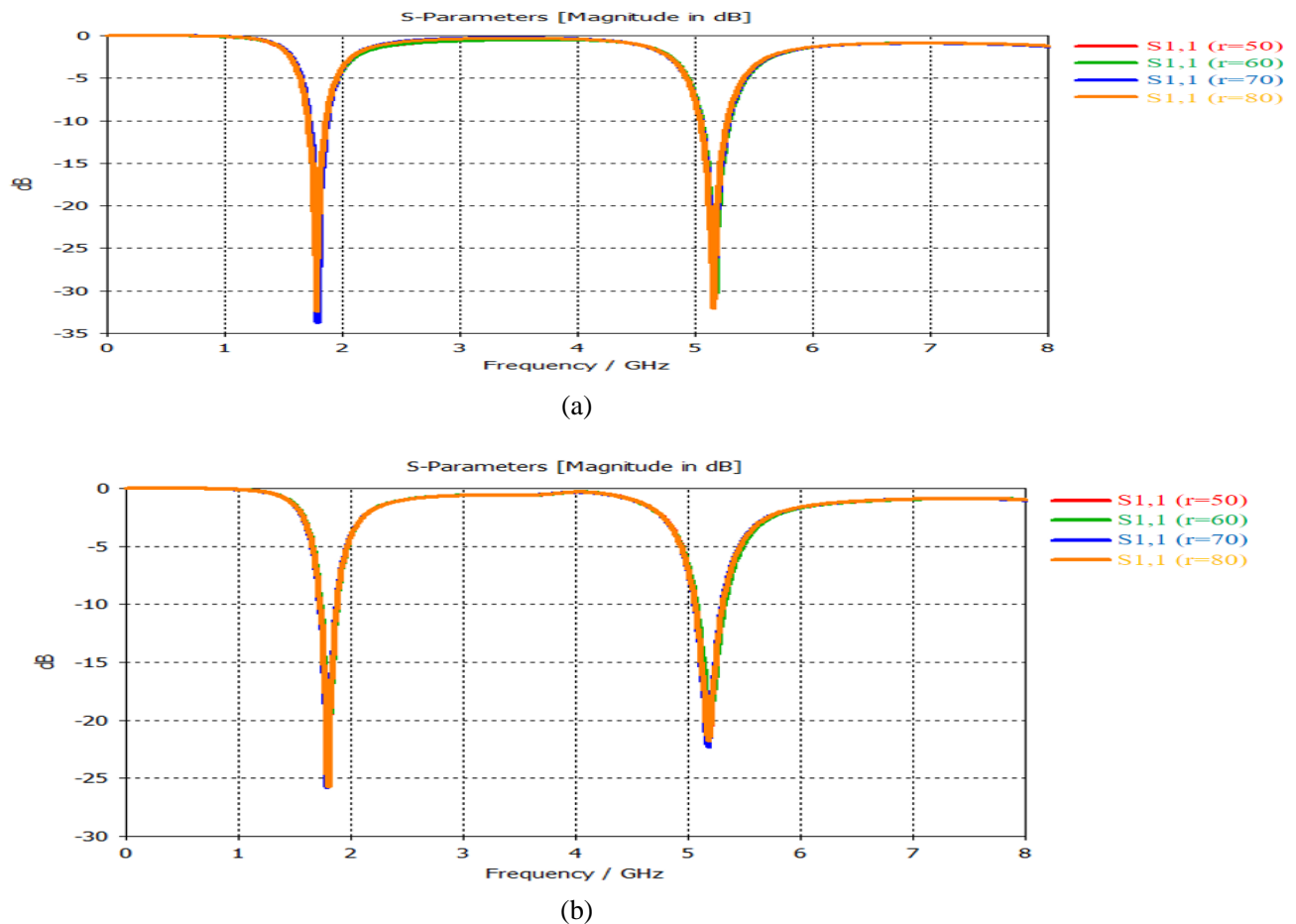


(a)



(b)

**Figure 17.** The reflection coefficients of antenna while bending at: (a) ($x$-axis) and (b) ($y$-axis).

**Table 5.** Simulated reflection coefficient, bandwidth and gain of the antenna at bending conditions with different radii at the $x$-axis.

| Cylindrical Bend ($r$) (mm) | Reflection Coefficient (dB) | | Bandwidth (GHz) | | Gain (dBi) | |
|---|---|---|---|---|---|---|
| | $fo_1 = 1.81$ GHz | $fo_2 = 5.2$ GHz | $fo_1 = 1.81$ GHz | $fo_2 = 5.2$ GHz | $fo_1 = 1.81$ GHz | $fo_2 = 5.2$ GHz |
| (planar) | −38.43 | −29.34 | 0.16 (1.73–1.89) | 0.25 (5.08–5.33) | 1.47 | 5.67 |
| $r = 50$ | −24.67 | −20.08 | 0.16 (1.71–1.87) | 0.24 (5.05–5.29) | 1.77 | 4.68 |
| $r = 60$ | −25.75 | −21.16 | 0.15 (1.71–1.86) | 0.24 (5.05–5.29) | 1.58 | 4.88 |
| $r = 70$ | −25.78 | −21.94 | 0.15 (1.72–1.87) | 0.24 (5.04–5.28) | 1.73 | 4.75 |
| $r = 80$ | −25.85 | −22.44 | 0.15 (1.72–1.87) | 0.24 (5.06–5.30) | 1.71 | 4.73 |

**Table 6.** Simulated reflection coefficient, bandwidth, and gain of the antenna at bending conditions with different radii at the $y$-axis.

| Cylindrical Bend ($r$) (mm) | Reflection Coefficient (dB) | | Bandwidth (GHz) | | Gain (dBi) | |
|---|---|---|---|---|---|---|
| | $fo_1 = 1.81$ GHz | $fo_2 = 5.2$ GHz | $fo_1 = 1.81$ GHz | $fo_2 = 5.2$ GHz | $fo_1 = 1.81$ GHz | $fo_2 = 5.2$ GHz |
| (planar) | −38.43 | −29.34 | 0.16 (1.73–1.89) | 0.25 (5.08–5.33) | 1.47 | 5.67 |
| $r = 50$ | −29.48 | −30.46 | 0.16 (1.71–1.87) | 0.24 (5.05–5.29) | 1.56 | 4.31 |
| $r = 60$ | −29.26 | −30.72 | 0.15 (1.71–1.86) | 0.24 (5.05–5.29) | 1.54 | 4.40 |
| $r = 70$ | −33.72 | −28.47 | 0.15 (1.72–1.87) | 0.24 (5.04–5.28) | 1.53 | 4.51 |
| $r = 80$ | −32.45 | −32.05 | 0.16 (1.70–1.86) | 0.23 (5.04–5.27) | 1.52 | 4.52 |

It was bent at radii of 50 mm, 60 mm, 70 mm, and 80 mm over the $y$-axis and $x$-axis, as shown in Figure 16. Due to SMA connection stress on the opposite side, the integrated design was bent over one side only along the $x$-axis. It was also twisted along the $y$-axis on its neighboring sides. Figure 17 shows the proposed antenna's simulated reflection coefficient when it is analyzed under bending in free space. According to simulation results, antenna bending along both the $x$-axis and $y$-axis reduces the reflection coefficient value of the antenna without changing the antenna's resonant frequency. This is due to smaller variations in the antenna's apparent length. Tables 5 and 6 show the bending analysis bandwidth, gain, and resonant frequency information at the $x$-axis and $y$-axis, respectively.



(a)                              (b)
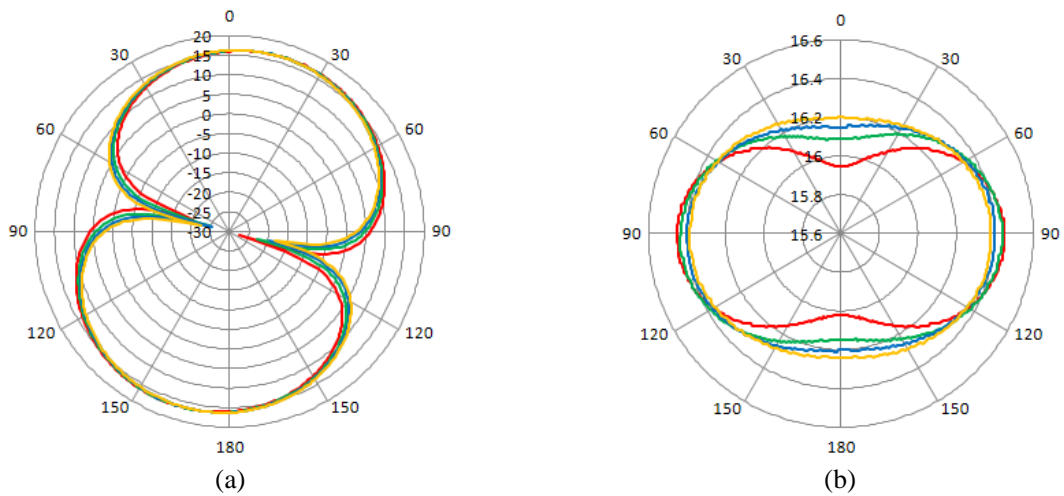
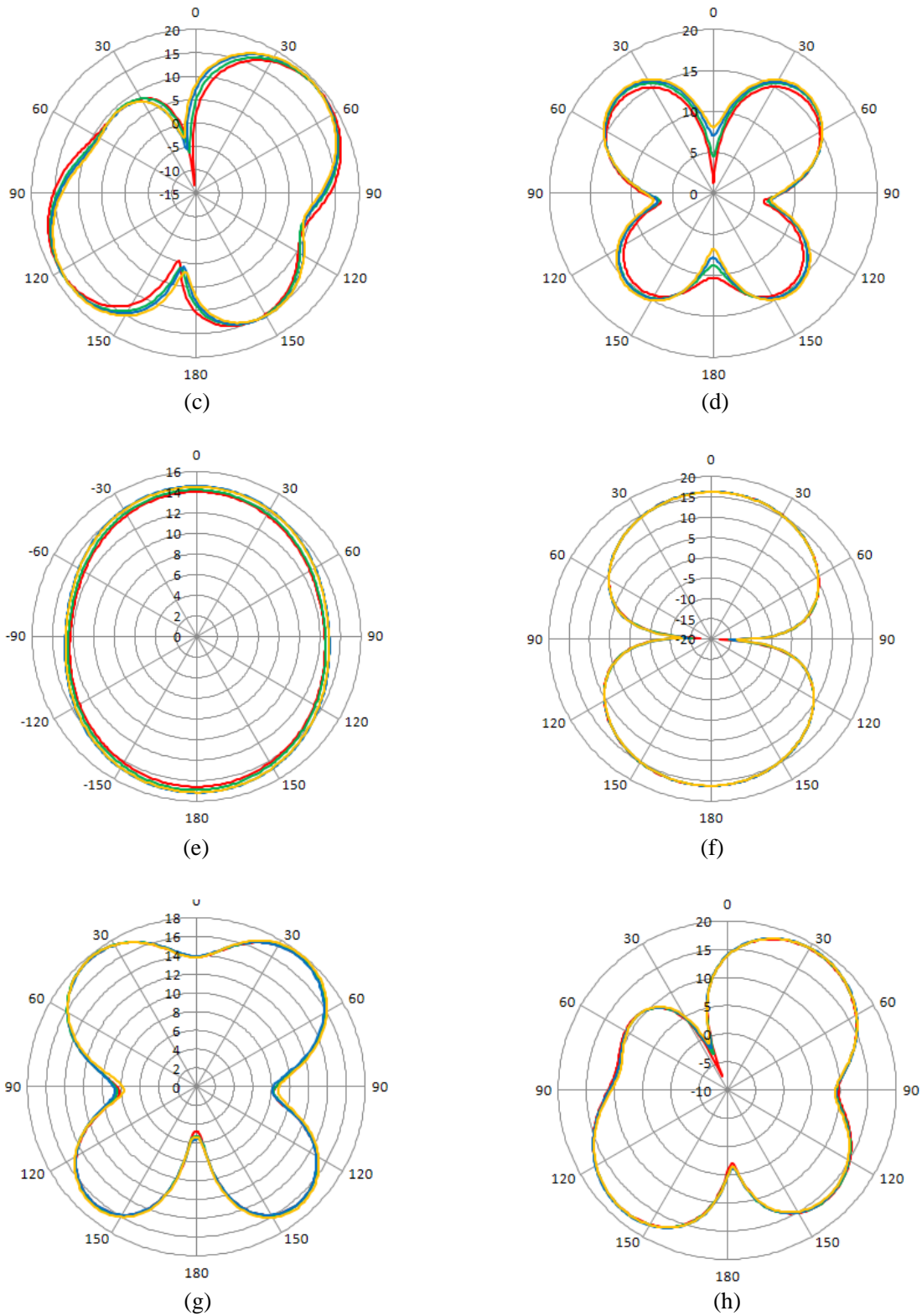**Figure 18.** Simulated radiation patterns of the proposed antenna when bent at the (a) $x$-axis (phi $= 0°$) at (1.81 GHz), (b) $x$-axis (phi $= 90°$) at (1.81 GHz), (c) $x$-axis (phi $= 0°$) at (5.2 GHz), (d) $x$-axis (phi $= 90°$) at 5.2 GHz, (e) $y$-axis (phi $= 0°$) at 1.81 GHz, (f) $y$-axis (phi $= 90°$) at (1.81 GHz), (g) $y$-axis (phi $= 0°$) at (5.2 GHz) and (h) $y$-axis (phi $= 90°$) at (5.2 GHz).

The simulated radiation patterns for frequency bands 1.81 GHz and 5.2 GHz for bending radii of $r = 50$ mm, 60 mm, 70 mm, and 80 mm in the ($x$-axis and $y$-axis) are shown in Figure 18. The radiation patterns are shown at Phi = 0° and Phi = 90°. In Figures 18(a)–(d), at 1.81 GHz, the antenna seems to have an omnidirectional pattern in the Phi = 0° and a dipole-like pattern in the Phi = 90°. Meanwhile, the antenna has a dipole-type pattern in Phi = 0° and a directional pattern in Phi = 90° at 5.2 GHz. The patterns at the $y$-axis, Figures 18(e)–(h), show a dipole-like pattern in the Phi = 0° and an omnidirectional pattern in the Phi = 90° at 1.81 GHz while at 5.2 GHz, the patterns show a dipole-like pattern in the Phi = 0° and an omnidirectional pattern in the Phi = 90°. Based on that, the bending of the antenna at both the $x$-axis and $y$-axis does not lead to a significant change in the radiation pattern.

# 7. CONCLUSION

In this paper, a flexible tree-shaped fractal antenna fed by a microstrip feed is proposed to fulfill dual-band wearable application requirements. The antenna is only 0.25 mm thick, making it suitable for the use as a wearable device with a sufficient range of flexibility. The resultant antenna offers two resonating bands with acceptable radiation patterns and gain. The lower resonating band ranges from 1.72 to 1.88 GHz with a center frequency of 1.81 GHz at $S_{11}$ of $-33$ dB, and the upper resonating band from 5.08 to 5.33 GHz with a center frequency of 5.2 GHz at $S_{11}$ of $-34.8$ dB. The antenna's resonance frequency, bandwidth, and gain for both bands are unaffected by bending along the $lx$-axis and $ly$-axis. The radiation patterns show that the antenna worked effectively before and after bending. According to the results of the study, the presented antenna could be considered a promising contender for existing wearable devices.

## REFERENCES

1. Manna, S., T. Bose, and R. Bera, "Wearable antennas for medical application: A review," *Advances in Electronics, Communication and Computing*, 115–130, Springer, Berlin, Germany, 2018, doi: 10.1007/978-981-10-4765-7_13.

2. Lee, H., J. Tak, and J. Choi, "Wearable antenna integrated into military berets for indoor/outdoor positioning system," *IEEE Antennas and Wireless Propagation Letters*, Vol. 16, 1919–1922, Mar. 2017, doi: 10.1109/LAWP.2017.2688400.

3. Paracha, K. N., S. K. A. Rahim, P. J. Soh, and M. Khalily, "Wearable antennas: A review of materials, structures, and innovative features for autonomous communication and sensing," *IEEE Access*, Vol. 7, 2019, doi: 10.1109/ACCESS.2019.2909146.

4. Dey, A. B., D. Mitra, and W. Arif, "Design of CPW fed multiband antenna for wearable wireless body area network applications," *International Journal of RF and Microwave Computer-aided Engineering*, Vol. 30, No. 12, 2020, https://doi.org/10.1002/mmce.22459.

5. Yan, S. and G. A. E. Vandenbosch, "Radiation pattern-reconfigurable wearable antenna based on metamaterial structure," *IEEE Antennas and Wireless Propagation Letters*, Vol. 15, 1715–1718, 2016, doi: 10.1109/LAWP.2016.2528299.

6. Yassen, M. T., M. R. Hussan, H. A. Hammas, A. J. Salim, and J. K. Ali, "Design of compact dual-band fractal monopole antenna with virtually extended ground plane," *Advanced Electromagnetics*, Vol. 7, No. 4, Aug. 2018, doi: https://doi.org/10.7716/aem.v7i4.725.

7. Kazerooni, H. and A. Khavasi, "Plasmonic fractals: Ultrabroadband light trapping in thin film solar cells by a Sierpinski nanocarpet," *Opt. Quant. Electron.*, 2013, doi: 10.1007/s11082-013-9783-0.

8. Jafari, H., H. Heidarzadeh, G. Rostami, M. Dolatyari, and A. Rostami, "Continuous terahertz wave generation based on photomixers coupled to Fibonacci fractal tree antennas," *Opt. Quant. Electron.*, 2016, doi: 10.1007/s11082-016-0810-9.

9. Arif, A., M. Zubair, M. Ali, M. U. Khan, and M. Q. Mehmood, "A compact, low-profile fractal antenna for wearable on-body WBAN applications," *IEEE Antennas and Wireless Propagation Letters*, Vol. 18, No. 5, 981–985, May 2019, doi: 10.1109/LAWP.2019.2906829.

10. Wang, L., J. Yu, T. Xie, and K. Bi, "A novel multiband fractal antenna for wireless application," *International Journal of Antennas and Propagation*, Vol. 2021, Article ID 9926753, 9 pages, 2021, https://doi.org/10.1155/2021/9926753.

11. Zhou, Z., W. Liao, Q. Zhang, F. Han, and Y. Chen, "A multi-band fractal antenna for RF energy harvesting," *2016 IEEE International Symposium on Antennas and Propagation (APSURSI)*, Fajardo, PR, USA, 2016, doi: 10.1109/APS.2016.7696017.

12. Weng, W.-C. and C.-L. Hung, "An H-fractal antenna for multiband applications," *IEEE Antennas and Wireless Propagation Letters*, 2014, doi: 10.1109/LAWP.2014.2351618.

13. Roushdy, M. M. and H. F. Hammad, "Inkjet printed wearable Hilbert monopole fractal antenna optimized for BAN systems," *National Radio Science Conference*, Aswan, Egypt, Feb. 22–25, 2016, doi: 10.1109/NRSC.2016.7450817.

14. Petkov, P. Z. and B. G. Bonev, "Analysis of a modified Sierpinski Gasket antenna for Wi-Fi aplications," *24th International Conference Radioelektronika*, 2014, doi: 10.1109/Radioelek.2014.6828489.

15. Elavarasi, C. and T. Shanmuganantham, "Multiband SRR loaded Koch star fractal antenna," *Alexandria Engineering Journal*, Vol. 57, 1549–1555, 2018, https://doi.org/10.1016/j.aej.2017.04.001.

16. Ali, J., S. Abdulkareem, A. Hammoodi, A. Salim, M. Yassen, M. Hussan, and H. Al-Rizzo, "Cantor fractal-based printed slot antenna for dual-band wireless applications," *International Journal of Microwave and Wireless Technologies*, Vol. 8, No. 2, 263–270, Mar. 2016, doi: https://doi.org/10.1017/S1759078714001469.

17. Silva Neto, V. P. and A. G. D'Assunção, "Iterative full-wave analysis of mandelbrot-inspired fractal patch antenna on textile substrate for UWB applications," *International Journal of Antennas and Propagation*, Vol. 2017, Article ID 4686315, 6 pages, 2017, https://doi.org/10.1155/2017/4686315.

18. Biswas, B., R. Ghatak, and D. R. Poddar, "A Fern fractal leaf inspired wideband antipodal vivaldi antenna for microwave imaging system," *IEEE Transactions on Antennas and Propagation*, 2017, doi: 10.1109/TAP.2017.2748361.

19. Hatem, G. M., A. J. Salim, T. A. Elwi, H. T. Ziboon, J. H. Majeed, and J. K. Ali, "Wunderlich fractal-based printed dual-band dipole antenna for wearable RFID applications," *Journal of Engineering and Applied Sciences*, Vol. 14. No. 4, 1093–1099, 2019, doi: 10.36478/jeasci.2019.1093.1099.

20. Ahmed, M. I. and M. F. Ahmed, "Fractal antennas for wearable applications," *Fractal Analysis*, 2018, Intechopen, doi: 10.5772/intechopen.81503.

21. Barreto, E. L. and L. M. Mendonça, "A new triple band microstrip fractal antenna for C-band and S-band applications," *Journal of Microwaves, Optoelectronics and Electromagnetic Applications*, Vol. 15, No. 3, 2016, doi: 10.1590/2179-10742016v15i3543.

22. Hatem, G. M., A. J. Salim, and J. K. Ali, "Wearable Sierpinski dragon fractal patch antenna for RFID applications," *International Conference on Engineering Sciences Applications*, Dec. 2014, doi: 10.13140/RG.2.1.3647.1529.

23. Silva Junior, P. F., E. E. C. Santana, M. S. S. Pinto, R. C. S. Freire, M. A. Oliveira, G. Fontgalland, and P. H. F. Silva, "Flexible wearable pre-fractal antennas for personal high-temperature monitoring," *Wireless Personal Communications*, Vol. 114, 1983–1998, 2020, https://doi.org/10.1007/s11277-020-07458-0.

24. Sran, S. S. and J. S. Sivia, "ANN and IFS based wearable hybrid fractal antenna with DGS for S, C and X band application," *International Journal of Electronics and Communications*, Aug. 2020, https://doi.org/10.1016/j.aeue.2020.153425.

25. Sahni, S., V. Gupta, and S. Negi, "Design and simulation of pythagorean tree monopole fractal antenna," *International Journal of Scientific & Engineering Research*, Vol. 6, No. 1, Jan. 2015.

26. Shrestha, S., S. R. Le, and D.-Y. Choi, "A new fractal-based miniaturized dual band patch antenna for RF energy harvesting," *International Journal of Antennas and Propagation*, Vol. 2014, Article ID 805052, 9 pages, 2014, https://doi.org/10.1155/2014/805052.

27. Stevens, R. T., *Fractal Programming in C*, M&T Books, Redwood City, CA, 1989.

28. Sreelakshmy, R., S. Ashok Kumar, and T. Shanmuganantham, "A wearable type embroidered logo antenna at ISM band for military applications," *Microwave and Optical Technology Letters*, Vol. 59, 2159–2163, 2017.

29. Seman, F. C., F. Ramadhan, N. S. Ishak, R. Yuwono, Z. Z. Abidin, S. H. Dahlan, S. M. Shah, and A. Y. I. Ashyap, "Performance evaluation of a star-shaped patch antenna on polyimide film under various bending conditions for wearable applications," *Progress In Electromagnetics Research Letters*, Vol. 85, 125–130, 2019.

30. Mandal, D. and S. S. Pattnaik, "Quad-band wearable slot antenna with low SAR values for 1.8 GHz DCS, 2.4 GHz WLAN and 3.6/5.5 GHz WiMAX applications," *Progress In Electromagnetics Research B*, Vol. 81, 163–182, 2018.

31. Hamouda, Z., J.-L. Wojkiewicz, A. A. Pud, L. Koné, S. Bergheul, and T. Lasri, "Magnetodielectric nanocomposite polymer-based dual-band flexible antenna for wearable applications," *IEEE Transactions on Antennas and Propagation*, Vol. 66, 3271–3277, 2018.